# Computer simulation results for bounds on the effective conductivity of composite media

P. A. Smith
*Department of Mechanical and Aerospace Engineering, North Carolina State University, Raleigh, North Carolina 27695-7910*

S. Torquato[a)]
*Departments of Mechanical and Aerospace Engineering and of Chemical Engineering, North Carolina State University, Raleigh, North Carolina 27695-7910*

(Received 25 July 1988; accepted for publication 7 October 1988)

This paper studies the determination of third- and fourth-order bounds on the effective conductivity $\sigma_e$ of a composite material composed of aligned, infinitely long, identical, partially penetrable, circular cylinders of conductivity $\sigma_2$ randomly distributed throughout a matrix of conductivity $\sigma_1$. Both bounds involve the microstructural parameter $\zeta_2$ which is a multifold integral that depends upon $S_3$, the three-point probability function of the composite. This key integral $\zeta_2$ is computed (for the possible range of cylinder volume fraction $\phi_2$) using a Monte Carlo simulation technique for the penetrable-concentric-shell model in which cylinders are distributed with an arbitrary degree of impenetrability $\lambda$, $0 \leqslant \lambda \leqslant 1$. Results for the limiting cases $\lambda = 0$ ("fully penetrable" or randomly centered cylinders) and $\lambda = 1$ ("totally impenetrable" cylinders) compare very favorably with theoretical predictions made by Torquato and Beasley [Int. J. Eng. Sci. **24**, 415 (1986)] and by Torquato and Lado [Proc. R. Soc. London Ser. A **417**, 59 (1988)], respectively. Results are also reported for intermediate values of $\lambda$: cases which heretofore have not been examined. For a wide range of $\alpha = \sigma_2/\sigma_1$ (conductivity ratio) and $\phi_2$, the third-order bounds on $\sigma_e$ significantly improve upon second-order bounds which just depend upon $\phi_2$. The fourth-order bounds are, in turn, narrower than the third-order bounds. Moreover, when the cylinders are highly conducting ($\alpha \gg 1$), the fourth-order lower bound provides an excellent estimate of the effective conductivity for a wide range of volume fractions.

## I. INTRODUCTION

The problem of predicting effective parameters (e.g., transport, mechanical, and electromagnetic properties) of disordered composite media is of great fundamental and practical importance and has received considerable attention in recent years.[1-3] From a design as well as a theoretical standpoint, it is desirable to calculate the effective property from a knowledge of the microstructure of the composite material; one can then systematically relate changes in the microstructure quantitatively to changes in the macroscopic variables. Unfortunately, in order to exactly predict the effective parameter, an infinite set of correlation functions, which statistically characterize the microstructure, must be known.[4,5] Except for a few special cases, the infinite set of correlation functions is never known and hence an exact determination of the effective property, for all phase property values and volume fractions, is generally out of the question, even for simple random models (e.g., random arrays of parallel cylinders or spheres).

Rigorous bounding methods, however, provide a means of estimating the effective parameter given a *limited* amount of microstructural information on the composite. Rigorous upper and lower bounds are useful because: (1) They enable one to test the relative merits of a theory or computer-simulation experiment for the property of interest; (2) the bounds become progressively narrower as more microstructural information is incorporated; and (3) one of the bounds can typically provide a relatively accurate estimate of the property even when the reciprocal bound diverges from it.[2]

In this article, we consider the evaluation of bounds on the effective transverse thermal (electrical) conductivity $\sigma_e$ of models of transversely isotropic fiber-reinforced materials composed of two different materials (phases) having phase conductivities $\sigma_1$ and $\sigma_2$ and phase volume fractions $\phi_1$ and $\phi_2$. By "fiber-reinforced," we mean any material whose phase boundaries are cylindrical surfaces, with generators parallel to one axis.[6] Continuous glass, carbon, or graphite fibers are examples of composites that fall within this category.[1] This classification also includes thin films where films consisting of columns of one material in a matrix of another are observed.[7]

Given only $\sigma_1$, $\sigma_2$, and $\phi_2$, Hashin[6] has obtained the best possible bounds on the effective conductivity of transversely isotropic fiber-reinforced materials. Silnutzer[8] and Milton[4] have derived improved bounds which incorporate additional microstructural information, valid for any isotropic fiber-reinforced material. The Silnutzer bounds depend upon an integral $\zeta_2$ which involves the three-point probability function $S_3$, defined below. [The $n$-point probability function $S_n(\mathbf{r}_1,\ldots,\mathbf{r}_n)$ gives the probability of finding $n$ points with positions $\mathbf{r}_1,\ldots,\mathbf{r}_n$ simultaneously in one of the phases, say phase 1.] The Milton bounds depend not only on $\zeta_2$ but also upon an integral involving the four-point probability function $S_4$, which itself can be expressed solely in terms of $\phi_2$ and $\zeta_2$.[7] Thus, the key microstructural parameter which arises in

[a)] To whom all correspondence should be addressed.

 0021-8979/89/030893-08$02.40  

both the Silnutzer and Milton bounds is $\zeta_2$. Because $S_3$ has been difficult to determine either theoretically or experimentally, application of the Silnutzer and Milton bounds has been very limited. Recent theoretical and experimental advances in characterizing the microstructure of composite media has broken this impasse. Torquato and Stell[9] have developed a theoretical formalism for systematically representing and calculating the $S_n$ for random distributions of inclusions of particles, given the $n$-particle distribution functions $g_n$ which characterize the probability of finding any $n$ particles with a particular configuration. The $S_n$ are multidimensional integrals over the $g_n$. This analytical representation of the $S_n$ has enabled investigators to compute $\zeta_2$ and its three-dimensional counterpart[4] for nontrivial models of random composite media.[10–12] For example, Torquato and Lado[12] employed this formalism for the fiber-reinforced material composed of a distribution of infinitely long, parallel, impenetrable cylinders (impenetrable disks in two dimensions) and greatly simplified $\zeta_2$ (which involves up to ninefold integrals) by expanding angular-dependent terms in its integrand in Chebyshev polynomials; they found that

$$\zeta_2 = k_2\phi_2^2 + k_3\phi_2^3 , \tag{1}$$

where

$$k_2 = \pi R^2 \int_{2R}^{\infty} dr[rg_2(r)/(r^2 - R^2)^2] \tag{2}$$

and

$$k_3 = 4\sum_{n=2}^{\infty}(n-1)R^{2n-4}\int_0^{\infty}\frac{dr}{r^{n-1}}\int_0^{\infty}\frac{ds}{s^{n-1}} \times \int_0^{\pi} d\theta\,[g_3(r,s,\theta) - g_2(r)g_2(s)]T_n(\cos\theta). \tag{3}$$

Torquato and Lado[12] computed $k_2$ and $k_3$ for an equilibrium distribution of disks by employing the accurate Percus–Yevick approximation for the pair distribution function $g_2$ and, for lack of any more fundamental alternative, the Kirkwood superposition approximation[13]

$$g_3(r_{12},r_{13},r_{23}) = g_2(r_{12})g_2(r_{13})g_2(r_{23})$$

for the triplet distribution function. On the experimental side, Berryman[14] has, for the first time, implemented image processing techniques to measure $S_3$ of composite materials and evaluate $\zeta_2$.

Monte Carlo computer-simulation techniques have heretofore not been applied to obtain the integral $\zeta_2$ directly. This article reports such results for two-dimensional (2D) media composed of (possibly overlapping) identical disks of radius $R$ distributed throughout a matrix. (This is equivalent to a 3D distribution of parallel, infinitely long, equisized, circular cylinders.) As is well known in liquid-state theory, accurate simulations of three-point integrals of the type (3) or (8) are nontrivial because one must sample each realization for the three-point correlation function involved over all possible triangular shapes and sizes, and then average over all realizations.[15] Our simulation method makes use of some of the novel techniques employed by us to measure the two-point function $S_2$.[16]

Our interest in 2D media is twofold. First, certain 2D media (such as distributions of impenetrable disks) are useful models of fiber-reinforced materials. Second, since the salient qualitative behavior of the D-dimensional $\zeta_2$ is not strongly affected by a change in the dimensionality of the composite,[10–12] simulation results obtained for 2D models (which are less costly than 3D simulations) can be utilized to infer the qualitative behavior of $\zeta_2$ for analogous 3D models. Our simulation technique, moreover, is easily extended to 3D media.

In this investigation, we seek to study the effect of interparticle connectedness on $\zeta_2$, and hence on effective conductivity bounds, for isotropic distributions of cylinders in the penetrable-concentric-shell (PCS) model introduced by Torquato.[17] The degree of the connectivity of the phases may dramatically influence transport and mechanical properties of multiphase media, particularly when one of the phase properties differs significantly.[17,18] Interparticle connectedness in the PCS model is a function of the degree of impenetrability $\lambda(0\leqslant\lambda\leqslant 1)$ of the disks; $\lambda = 0$ and $\lambda = 1$ corresponding to the limiting cases of "fully penetrable" and "totally impenetrable" cylinders, respectively. Note that the special case $\lambda = 1$ in the PCS model is exactly the same model employed in the analytical investigation of Torquato and Lado in which they found $\zeta_2$ to be given by Eq. (1). Thus, computer simulations of $\zeta_2$ for $\lambda = 1$ can be used to test the accuracy of using the Kirkwood superposition approximation for $g_3$ in integrals such as Eq. (3).

This paper is organized as follows. In Sec. II, we present and discuss the Silnutzer and Milton bounds on the effective transverse conductivity $\sigma_e$. In Sec. III, we describe our model system. In Sec. IV, we present our Monte Carlo method for computing $\zeta_2$. This is followed by a presentation in Sec. V of our results for $\zeta_2$ for distributions of cylinders in the PCS model at $\lambda = 0$, 0.7, 0.9, and 1, and at selected values of the cylinder volume fraction $\phi_2$. Finally, in Sec. VI, we present our evaluation of the Silnutzer and Milton bounds on $\sigma_e$ as a function of $\phi_2$ for various values of the impenetrability index $\lambda$.

## II. THIRD- AND FOURTH-ORDER BOUNDS

Given $\sigma_1$, $\sigma_2$, $\phi_2$, and two integrals involving certain three-point correlation functions, rigorous bounds on the effective conductivity $\sigma_e$ of any fiber-reinforced material, statistically isotropic in the transverse plane, have been derived by Silnutzer.[8] Milton[7] showed that the Silnutzer bounds may be expressed in terms of $\sigma_1$, $\sigma_2$, $\phi_2$, and a single integral $\zeta_2$ (defined below) which depends upon the three-point probability function described in Sec. I. The simplified form of the Silnutzer bounds are given by

$$\sigma_L^{(3)} \leqslant \sigma_e \leqslant \sigma_U^{(3)} , \tag{4}$$

where

$$\sigma_U^{(3)} = \left(\langle\sigma\rangle - \frac{\phi_1\phi_2(\sigma_2-\sigma_1)^2}{\langle\tilde{\sigma}\rangle + \langle\sigma\rangle_\zeta}\right) \tag{5}$$

and

$$\sigma_L^{(3)} = \left(\langle 1/\sigma\rangle - \frac{\phi_1\phi_2(1/\sigma_2 - 1/\sigma_1)^2}{\langle 1/\tilde{\sigma}\rangle + \langle 1/\sigma\rangle_\zeta}\right)^{-1} . \tag{6}$$

Here $\langle a\rangle = a_1\phi_1 + a_2\phi_2$, $\langle \tilde{a}\rangle = a_1\phi_2 + a_2\phi_1$, and $\langle a\rangle_\zeta = a_1\zeta_1 + a_2\zeta_2$, where $a$ represents any property. The microstructural parameters are related to one another by

$$\zeta_2 = 1 - \zeta_1, \tag{7}$$

where

$$\zeta_2 = \frac{4}{\pi\phi_1\phi_2}\int_0^\infty \frac{dz}{z}\int_0^\infty \frac{dy}{y}\int_0^\pi d\theta\, \hat{S}_3(y,z,\theta)\cos 2\theta \tag{8}$$

and

$$\hat{S}_3(y,z,\theta) = S_3(y,z,\theta) - S_2(y)S_2(z)/\phi_1. \tag{9}$$

The quantities $S_2(x)$ and $S_3(y,z,\theta)$ are, respectively, the probabilities of finding in phase 1 the end points of a line segment of length $x$ and the vertices of a triangle with sides of length $x$, $y$, and $z$; $\theta$ is the angle opposite the side of length $x$. The bounds (4) are exact through third order in $(\sigma_2 - \sigma_1)$ and hence are referred to as third-order bounds. The fact that $\zeta_2$ (or $\zeta_1$) lies in the interval $[0,1]$ implies that the Silnutzer bounds always improve upon the corresponding second-order bounds of Hashin.[6] Milton[7] has derived fourth-order bounds on $\sigma_e$ which depend not only upon $\sigma_1$, $\sigma_2$, and $\zeta_2$, but also upon a multidimensional integral that depends on the four-point probability function $S_4$. Utilizing a phase-interchange theorem for fiber-reinforced materials, Milton showed that the microstructural parameter involving $S_4$ can be expressed in terms of $\phi_2$ and $\zeta_2$ only. Milton's fourth-order bounds for transversely isotropic materials, for the case $\sigma_2 \geqslant \sigma_1$, are given by

$$\sigma_L^{(4)} \leqslant \sigma_e \leqslant \sigma_U^{(4)}, \tag{10}$$

where

$$\sigma_U^{(4)} = \sigma_2\left(\frac{(\sigma_1+\sigma_2)(\sigma_1+\langle\sigma\rangle) - \phi_2\zeta_1(\sigma_2-\sigma_1)^2}{(\sigma_1+\sigma_2)(\sigma_2+\langle\tilde{\sigma}\rangle) - \phi_2\zeta_1(\sigma_2-\sigma_1)^2}\right) \tag{11}$$

and

$$\sigma_U^{(4)} = \sigma_1\left(\frac{(\sigma_1+\sigma_2)(\sigma_2+\langle\sigma\rangle) - \phi_1\zeta_2(\sigma_2-\sigma_1)^2}{(\sigma_1+\sigma_2)(\sigma_1+\langle\tilde{\sigma}\rangle) - \phi_1\zeta_2(\sigma_2-\sigma_1)^2}\right). \tag{12}$$

The fact that the bounds diverge in the cases where the phase conductivities are widely different does not mean the bounds have no utility in such instances. Torquato[5] has observed that lower-order *lower* bounds (such as second-, third-, and fourth-order bounds) should provide good estimates of $\sigma_e/\sigma_1$ for $\alpha \gg 1$, provided that the volume fraction of the highly conducting phase $\phi_2$, is below its percolation-threshold value $\phi_{2c}$ and that the mean cluster size of phase 2, $\Lambda_2$, is much smaller than the macroscopic dimension of the sample $L$. (A cluster of phase $i$ is defined as that part of phase $i$ which can be reached from a point in phase $i$ without touching any part of phase $j, i \neq j$.) The accuracy of the lower-order lower bound, of course, increases as the order increases. Clearly, the condition $\Lambda_2 \ll L$ by itself implies that $\phi_2 < \phi_{2c}$. For periodic as well as random arrays of cylinders, the condition $\Lambda_2 \ll L$ is satisfied for all $\phi_2$, except at the close packing value for such systems, i.e., $\phi_2 = \phi_{2c}$. Similarly, lower-order *upper* bounds on $\sigma_e/\sigma_1$ for $\alpha \gg 1$ should yield useful estimates of $\sigma_e$, given that $\phi_2 > \phi_{2c}$ and $\Lambda_1 \ll L$, where $\Lambda_1$ is the mean cluster size of phase 1.

## III. MODEL SYSTEM

We consider computing $\zeta_2(\phi_2,\lambda)$ for isotropic distributions of equisized, parallel cylinders (or disks) at number density $\rho$ in the PCS model.[17] If phase 1 denotes the matrix phase, then $\phi_1$ is the matrix volume fraction, $\phi_2$ is the particle phase (or simply disk) volume fraction, and $S_3(y,z,\theta)$ gives the probability of finding the three vertices of a triangle with sides of length $y$ and $z$ and included angle $\theta$ all in the matrix phase. In the PCS model (depicted in Fig. 1), disks (or parallel cylinders) of radius $R$ are statistically distributed throughout a matrix subject only to the condition of a mutually impenetrable core of radius $\lambda R$; $\lambda$ being the impenetrability parameter, $0 \leqslant \lambda \leqslant 1$. Each disk of radius $R$, therefore, is composed of an impenetrable core of radius $\lambda R$, encompassed by a perfectly penetrable concentric shell of thickness $(1-\lambda)R$. It is clear that the limiting cases $\lambda = 0$ and $\lambda = 1$ correspond, respectively, to "fully penetrable" disks (in which disk centers are completely uncorrelated) and "totally impenetrable" disks. The PCS model with $\lambda \sim 1$ serves as a useful model of fiber-reinforced materials with oriented, continuous fibers and of thin films.[12] The 3D analog of the PCS model (involving spheres) for $\lambda < 1$ is a good model of consolidated media such as sandstones and sintered materials.[2]

For $\lambda > 0$ (i.e., for finite-sized hard cores), the impenetrability condition alone does not uniquely determine the distribution. Either an equilibrium distribution[13] or some nonequilibrium distribution, such as random sequential addition (RSA)[19] may be assumed. The equilibrium and RSA distributions are known to be different at sufficiently high density $\rho$ and $\lambda$.[19] For small enough $\rho$ and $\lambda$, the two are the same. Computer simulation results reported are for RSA.

RSA configurations are generated by placing particles in a unit cell randomly and sequentially. When each particle is added, it is determined whether its hard core (of radius $\lambda R$) overlaps any other hard core already in the unit cell; if

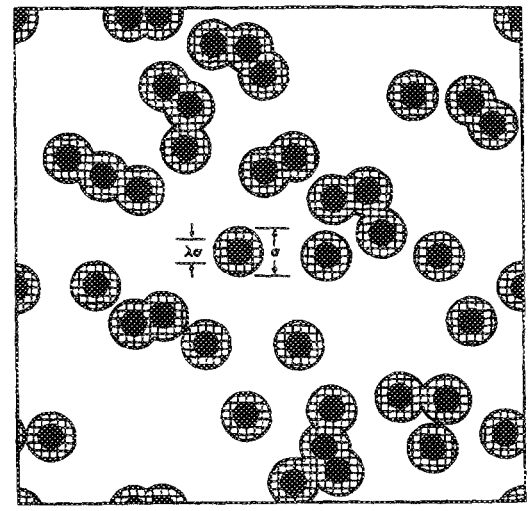


FIG. 1. A computer-generated realization of a distribution of disks of radius $R = \sigma/2$ (shaded region) in a matrix (unshaded region) in the PCS model (see Ref. 17). The disks have an impenetrable core of diameter $\lambda\sigma$ indicated by the smaller, black circular regions. Here $\lambda = 0.5$ and the particle volume fraction $\phi_2 = 0.3$.

so, that particular particle is removed and added again until it finds a vacancy. Ultimately, so many particles have been added that the next particle finds no accessible space (the *jammed* state). The jamming limit for RSA distributions of totally impenetrable disks ($\lambda = 1$) occurs at $\phi_2 \approx 0.55$,[16,20] which is well below the close-packing limit of $\phi_2 \approx 0.81$[12] for equilibrium distributions. Widom[19] discusses the differences between equilibrium and RSA distributions of particles for the case $\lambda = 1$ only. At low to moderate densities for $\lambda = 1$, the distributions are exactly the same. More precisely, equilibrium and RSA distributions are identical up through the level of the third virial coefficient. Practically, this means the distributions for 2D media with $\lambda = 1$ are virtually indistinguishable up to $\phi_2 \approx 0.4$.[16,21] At higher volume fractions, exclusion volume effects cause the RSA- and equilibrium-gap distributions to become very different, especially close to the RSA jamming limit. Since the two distributions for $\lambda = 1$ are essentially the same up to $\phi_2 \approx 0.4$, we shall compare our simulation results for this case to the analytical results of Torquato and Lado for equilibrium distributions of rigid disks and comment on the accuracy of the Kirkwood superposition approximation which they employ.

As the impenetrability index $\lambda$ is made smaller, the differences between the equilibrium and RSA distributions at fixed $\rho$ diminishes. Indeed, for the special case of fully penetrable disks ($\lambda = 0$), the two distributions are identical at any density since the distribution is uniquely determined by virtue of the total lack of spatial correlation between disk centers. In this limit, the $n$-point matrix probability functions have an especially simple analytical form. For example, for a distribution of fully penetrable disks at reduced number density $\eta = \rho A_1$ (where $A_1 = \pi R^2$ is the area of one disk), the $n$-point functions are given by[11]

$$S_n(\mathbf{r}_1,...,\mathbf{r}_n) = \exp[-\eta A_n(\mathbf{r}_1,...,\mathbf{r}_n)/A_1], \tag{13}$$

where $A_n(\mathbf{r}_1,...,\mathbf{r}_n)$ is the union volume of $n$ disks of diameter $\sigma = 2R$ with center coordinates given by $(\mathbf{r}_1,...,\mathbf{r}_n)$.

## IV. SIMULATION PROCEDURE

### A. Preliminary discussion

Consider rewriting the three-point integral $\zeta_2$ Eq. (7), as follows:

$$\zeta_2 = 1 - \frac{4}{\pi\phi_1\phi_2}\left\langle \int_0^\infty \frac{dz}{z}\int_0^\infty \frac{dy}{y}\int_0^\pi d\theta\, X_3(y,z,\theta)\cos 2\theta \right\rangle, \tag{14}$$

where

$$X_3(\mathbf{r}_1,\mathbf{r}_2\mathbf{r}_3) = I(\mathbf{r}_1)I(\mathbf{r}_2)I(\mathbf{r}_3) - I(\mathbf{r}_2)I(\mathbf{r}_3)/\phi_1, \tag{15}$$

and $I(\mathbf{r})$ is the characteristic function of the matrix phase defined by

$$I(\mathbf{r}) = \begin{cases} 1, & \mathbf{r} \in \text{matrix phase} \\ 0, & \text{otherwise} \end{cases}. \tag{16}$$

Here angular brackets denote an ensemble average and therefore, the first three $n$-point probability functions are defined by

$$S_1(\mathbf{r}_1) = \langle I(\mathbf{r}_1)\rangle, \tag{17}$$

$$S_2(\mathbf{r}_1,\mathbf{r}_2) = \langle I(\mathbf{r}_1)I(\mathbf{r}_2)\rangle, \tag{18}$$

$$S_3(\mathbf{r}_1,\mathbf{r}_2,\mathbf{r}_3) = \langle I(\mathbf{r}_1)I(\mathbf{r}_2)I(\mathbf{r}_3)\rangle. \tag{19}$$

For statistically isotropic media, the $S_n$ depend upon the relative distances between the points and hence $S_1 = \phi_1$, $S_2(r_1,r_2) = S_2(y)$, $S_3(r_1,r_2,r_3) = S_3(y,z,\theta)$, where $y = |\mathbf{r}_2 - \mathbf{r}_1|$, $z = |\mathbf{r}_3 - \mathbf{r}_1|$, and $\theta$ is the included angle between the displacements $(\mathbf{r}_2 - \mathbf{r}_1)$ and $(\mathbf{r}_3 - \mathbf{r}_1)$.

Obtaining $\zeta_2$ from computer simulations is a three-step process. Initially, one must generate realizations of the random media. Subsequently, one samples each realization for the three-point function $X_3$ for values of $(y,z,\theta)$ specified by the technique of integration. Finally, one sums the properly weighted contributions and averages over the total number of realizations to obtain $\zeta_2$. We are specifically interested in obtaining $\zeta_2$ for RSA distributions of disks in the PCS model at specified disk volume fraction $\phi_2$ and impenetrability index $\lambda$.

In general, the methods available for storing images of configurations of particles are: (1) a bit-mapped (digitized) image, (2) an object-oriented approach (defined below), or (3) some hybrid of the preceding two methods. In each case, periodic boundary conditions (PBC) are employed in order to simulate an infinite system (the image is surrounded with replicas of itself).

When a bit-mapped approach is used, disks are "painted" onto a large square grid (pixel array) by setting all bits inside the disks (and hence in the particle phase) to 1. We will use the terms "bit" and "pixel" interchangeably, even though this is not necessarily the case. Initially, all bits are zeroed or "unset" (100% matrix phase). Note that only phase information is retained; the disks lose any individual identity. The error introduced when representing objects in this manner diminishes as we increase the number of pixels; however, there is a practical upper limit to the number of pixels that may be used. We have referred to this approach as the GRID method.[16]

When an object-oriented approach is used, the coordinates of the centers of each disk are stored (if the disks are of unequal size, then the radius of each disk must also be stored). Note that the particles retain their individual identities. We have referred to this approach as the "stored-configuration" (SC) method. Monte Carlo[22] and molecular dynamics[15] techniques used in the study of the liquid state are examples of the SC method.

Configuration generation is faster with the SC method than with the GRID method for circular disks, due to the overhead of testing and setting the large number of pixels used with the GRID method. Configuration sampling is much faster with the GRID method than with the SC method for circular disks. GRID method phase sampling is accomplished by determining what pixel a test point falls in (PBC are applied) and then testing the state of the bit corresponding to that pixel (0 or 1). SC method phase sampling is accomplished by determining whether a test point is inside any disk in the system, i.e., if the minimum distance (employing PBC) between a test point and any disk in the configuration is less than the radius of that disk then that point is in the particle phase (phase 2); otherwise the point lies in the

matrix phase (phase 1). One enhancement to the SC method is the "cell-list"[23]; only nearby disks are tested, reducing the number of distances that must be computed.

The essential difficulty with the GRID method is one of resolution. The GRID method clearly breaks down if sampling distances are of the order of the size of a pixel. There is no resolution difficulty with the SC method, but even with the "cell-list" enhancement we found it to be too slow for our large sampling requirements.

The method we employ in this study (hereafter referred to as the SC/GRID method) is a hybridization of all the above methods. Such a technique was recently used by Lee and Torquato[24] to accurately measure the porosity $\phi_1$ in the PCS model (for both 2D and 3D media) as a function of $\rho$ and $\lambda$. Two pixel arrays are maintained for GRID method sampling. The first contains disk "lower-bounds," i.e., only pixels that lie completely within disks are set. The second contains disk "upper-bounds," i.e., all pixels that contain any points inside disks are set. Any pixel which has a different value in the two arrays is termed a "boundary pixel." Any pixel which is not a "boundary pixel" is a "definite pixel," and can be used for a definite phase determination (particle phase if set, matrix phase if unset). For the small (resolution dependent) fraction of pixels that are "boundary pixels," the "cell-list" enhancement of the SC method is used to eliminate the uncertainty in the phase of the test point. Therefore, the SC/GRID method is nearly as fast as the simple GRID method, but has the ability to resolve small distances accurately. In addition, by counting the pixels in each GRID array, we have rigorous upper- and lower-bounds on the disk volume fraction, $\phi_2$. The mean of these two bounds is in excellent agreement with values of $\phi_2$ obtained by direct simulation (measuring the fraction of random test points that lie in phase 2), and thus provides a simple way of determining $\phi_2$.

### B. Simulation details

All simulations were performed using the SC/GRID method (with PBC) on a IBM 3081 computer. Depending on the value of $\phi_2$ and $\lambda$, we generate realizations using 150–600 particles in the unit cell. Each GRID image was stored in a separate $128\times1024$ character array (8-bit characters, therefore $1024\times1024$ bits). Storing each image required 128 kB. A multiplicative congruential random number generator with multiplier 16807 and modulus $2^{31}$-1 was used to both generate and sample configurations. This generator has good lattice statistics and relatively fast execution time.[25]

In Ref. 16, the simple GRID method was used to calculate the two-point probability function, $S_2(x)$; this method may also be extended to calculate the three-point probability function $S_3(y,z,\theta)$. Clearly, the simple GRID method cannot be used to obtain accurate values of these quantities whenever the distances involved are very small because of resolution difficulties. Because $\zeta_2$ is obtained by integrating $S_3(y,z,\theta)$, and the region of integration very near $(y,z)=(0,0)$ makes a substantial contribution to this integral (especially for $\lambda>0$), the simple GRID method (even with an increased image resolution of $4096\times4096$ pixels) could not be used and the SC/GRID method is used instead.

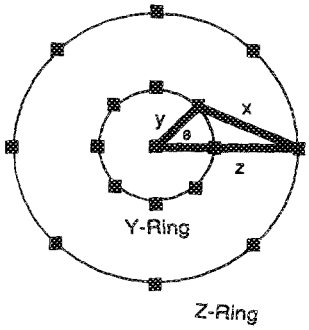


FIG. 2. A portion of a sampling template used in the ring method of integration. As illustrated, $N_\theta=5$, $N_z=1$, and $N_y=1$, for which 17 sampled points yield 64 nonredundant triangles. For the subregions of integration we examined in this study, we took $N_\theta=31$, $N_z=6$, and $N_y=4$, for which 1801 sampled points yield 86 400 nonredundant triangles.

For example, the innermost $y$-ring in the sampling template (Fig. 2) may map onto a single pixel; the innermost $z$-ring may map onto only a few pixels. If some of these pixels happen to be boundary pixels, great errors in $X_3(y,z,\theta)$ (and $\zeta_2$) will be introduced.

Instead of sampling and storing $X_3(y,z,\theta)$ values for a large number of triangles, performing ensemble averaging to obtain $\langle X_3(y,z,\theta)\rangle$, and then finally integrating to obtain $\zeta_2$ using Eq. (5), the approach of Eq. (14) was used. With this approach, integration is performed using the raw $X_3(y,z,\theta)$ values and the integral is then ensemble averaged. Gauss–Legendre quadrature is used for the $y$ and $z$ integrations; Simpson's rule is used for the $\theta$ integration. The use of Simpson's rule (which would not otherwise be used) is motivated by the need to have regular angular spacing; this permits a sampling template (a portion of which is shown in Fig. 2) to be used. When such a template is used, a large number of triangles [with the proper $(y,z,\theta)$ values for integration] can be constructed from a minimal set of sampled points. An analogous sampling template was used to sample for $S_2(r)$ in Ref. 16. The radial distances in the template are specified by the Gaussian integration method. The integration orders selected were: $N_z=6$, $N_y=4$, $N_\theta=31$. This specifies the number and location of points in the template.

One thousand sampling templates were sampled per generated configuration. Instead of adjusting the integration orders, the region of $y$-$z$ integration was subdivided until the specified orders produced convergent subintegrals. For impenetrable ($\lambda>0$) cases, the $y$-$z$ region of integration ($0<z<32R$, $0<y<z$) was subdivided into over 100 $y$-$z$ subregions. An initial estimate of each subintegral is made based on the value after five configurations. At that point, the subregions that contribute most to the integral are further sampled (ten more configurations are considered).

## V. RESULTS FOR THE THREE-POINT PARAMETER, $\zeta_2$

In Fig. 3 we present our evaluation of the three-point parameter $\zeta_2$ for distributions of parallel cylinders in the PCS model for $\lambda=0, 0.7, 0.9$, and 1, respectively, at selected values of the cylinder volume fraction $\phi_2$. The CPU time required to compute $\zeta_2$ for the $\lambda$ values was approximately 50 CPU hours.

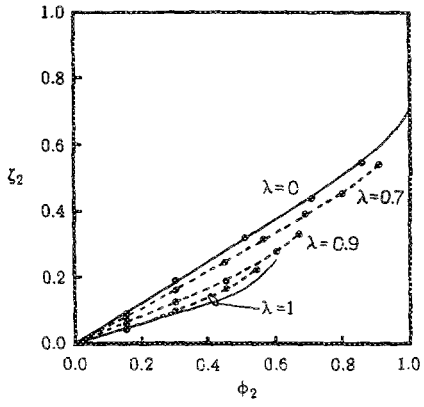


FIG. 3. RSA simulation results for the three-point parameter $\zeta_2$ in the PCS model at selected values of the impenetrability parameter $\lambda$. Also shown (solid lines) are exact results using Eq. (15) for the case $\lambda = 0$ and the corresponding equilibrium results of Torquato and Lado for the case $\lambda = 1$.

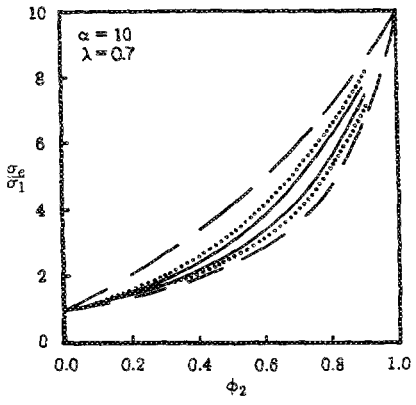


FIG. 4. Bounds on $\sigma_e/\sigma_1$ as a function of $\phi_2$ at $\alpha = 10$ and $\lambda = 0.7$ computed from $\zeta_2$ results presented in Fig. 3. Dashed lines, Hashin bounds; dotted lines, Silnutzer bounds; solid lines, Milton bounds.

For the case of fully penetrable disks ($\lambda = 0$), Torquato and Beasley[11] obtained $\zeta_2$ exactly using Eq. (13). Our results are in excellent agreement with their results; in fact, this case was used extensively during development of simulation methods as a test case. We obtained an rms deviation for the case $\lambda = 0$ of about 2%.

The results reported for $\lambda > 0$ are new, with the highest volume fractions shown corresponding the respective jamming-limit values.[16] For fixed $\phi_2$, $\zeta_2$ is a monotonically decreasing function of $\lambda$, as expected. The reason for such behavior is explained in Ref. 12. The three-point parameter is seen to be approximately linear for a wide range of volume fractions for all $\lambda$. As the jamming-limit is approached in each case where $\lambda > 0$, $\zeta_2$ characteristically rises faster than linearly in $\phi_2$ due to exclusion-volume effects.[12] However, because of gap distribution differences noted earlier, we expect this rise to be less pronounced for RSA distributions than for equilibrium distributions. For the case of totally impenetrable disks ($\lambda = 1$), we compare our results to those of Torquato and Lado[12] for an equilibrium distribution. Through second order in $\phi_2$, they exactly found

$$\xi_2 = \phi_2/3 - 0.05707\phi_2^2 + O(\phi_2^3). \tag{20}$$

Since RSA and equilibrium distributions are the same through the level of the third virial coefficient, then (20) is also exact for the RSA distribution. From Fig. 3, we see that our simulations for $\lambda = 1$ follow (20) closely for small $\phi_2$. The simulation agrees well with the Torquato–Lado results up to $\phi_2 = 0.3$, where our value is about 5% greater than the equilibrium value obtained using the Kirkwood superposition approximation. At $\phi_2 = 0.4$, the simulation is about 17% greater than the equilibrium result. Thus, in light of our aforementioned comments regarding the similarities between RSA and equilibrium distributions for $\phi_2 \leqslant 0.4$, this indicates that the superposition in (3) accurately gives $\zeta_2$ for lower concentrations ($\phi_2 < 0.3$) but underestimates $\zeta_2$ for the higher range $0.3 \leqslant \phi_2 \leqslant 0.4$. This is consistent with findings of the low-density analysis of Beasley and Torquato[26] for the 3D counterpart of $\zeta_2$. An underestimation of $\zeta_2$ (due to the use of the superposition approximation), in the case of conducting particles, for example, implies an underestimation of the lower bound and hence the use of such a $\zeta_2$ still provides a strict lower bound. For $\phi_2 > 0.4$, differences between the RSA and equilibrium distributions make it difficult to draw any conclusions about the accuracy of the superposition approximation.

Finally, it is to be noted that we very recently learned of a study by Sangani and Yao[27] in which the microstructural parameter $\zeta_2$ was indirectly determined from a computer simulation of an equilibrium distribution of totally impenetrable cylinders ($\lambda = 1$), i.e., they obtained $\zeta_2$ without directly evaluating the integral (8). They used 16–32 particles per unit cell; an order of magnitude less than we employed. For $\phi_2$ less than about 0.25, the two methods are in very good agreement. For $0.3 \leqslant \phi_2 \leqslant 0.4$, the range over which the RSA and equilibrium distributions are still expected to be essentially the same, $\zeta_2$ determined in Ref. 27 is lower than our corresponding estimates (e.g., our predictions at $\phi_2 = 0.3$ and 0.4 are, respectively, approximately 7% and 35% higher than their results). It is not clear whether their underestimation of $\zeta_2$ for this range of $\phi_2$ is due to the use of a much smaller number of particles per unit cell or to the indirect method they used to obtain it.

## VI. EVALUATION OF THIRD- AND FOURTH-ORDER BOUNDS ON $\sigma_e$

Utilizing the results for $\zeta_2$ of the previous section, the third- and fourth-order bounds were calculated using Eqs.

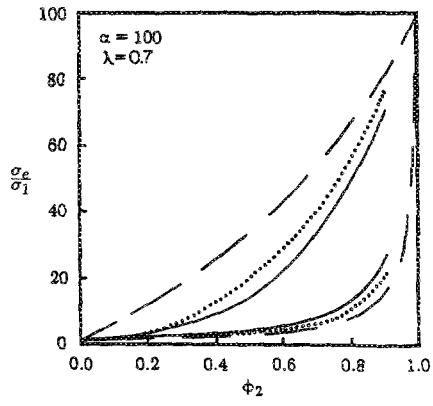


FIG. 5. As in Fig. 4, with $\alpha = 100$.

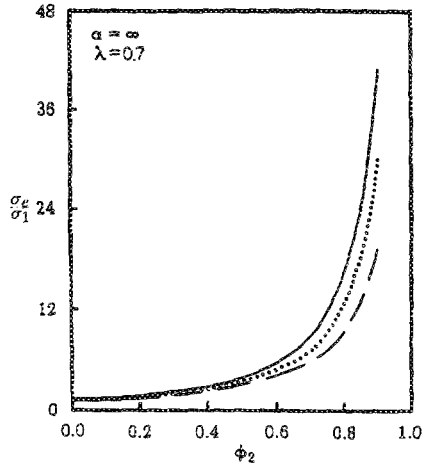


FIG. 6. As in Fig. 4, with $\alpha = \infty$. The upper bounds do not appear as they diverge to infinity in the limit $\alpha \ll \infty$. Milton's fourth-order lower bound, however, gives an excellent estimate of $\sigma_e/\sigma_1$, provided that the mean cluster size $\Lambda_2$ is much smaller than the macroscopic length of the sample $L$.

(4)–(12). We present in Figs. 4–6 plots of the Hashin, Silnutzer, and Milton bounds on the scaled conductivity $\sigma_e/\sigma_1$ as a function of the cylinder volume fraction $\phi_2$ for $\lambda = 0.7$ at values of the conductivity ratio $\alpha = 10$, 100, and $\infty$, respectively. In the sets of Figs. 7–9 and 10–12, we plot analogous bounds, respectively, for $\lambda = 0.9$ and $\lambda = 1.0$. The second-order Hashin bounds, which depend only on $\phi_2$ (and hence are independent of $\lambda$ and $\zeta_2$), are included for purposes of comparison. We see in each case that the second-order Silnutzer bounds are a major improvement over the Hashin bounds; the fourth-order Milton bounds are sharper still. Most of the improvement comes from the upper bounds.

The bounds, as expected, widen as $\alpha$ is increased from 10 to 100. As indicated earlier, this does not imply that the bounds have no utility in such instances. The fourth-order lower bounds, for example, will provide a useful estimate of $\sigma_e/\sigma_1$ provided that $\phi_2 < \phi_{2c}$ and $\Lambda_2 \ll L$. For the case $\lambda = 1$, these conditions will be met for all $\phi_2$ except at the jamming limit $\phi_2 \approx 0.545$ which also corresponds to $\phi_{2c}$. For $\lambda = 0.7$ and 0.9, the jamming-limit values lie above the percolation threshold values. An estimate of $\phi_{2c}$ for these latter two values of $\lambda$ can be determined from equilibrium simulations[28]

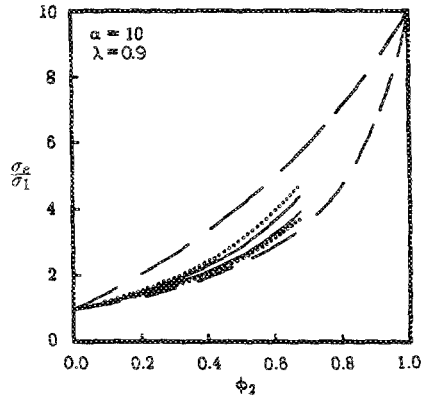


FIG. 7. As in Fig. 4, with $\lambda = 0.9$.

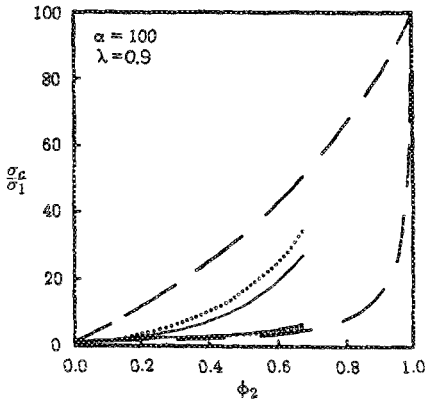


FIG. 8. As in Fig. 5, with $\lambda = 0.9$.

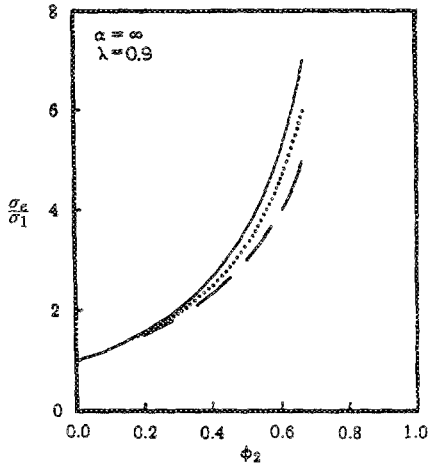


FIG. 9. As in Fig. 6, with $\lambda = 0.9$.

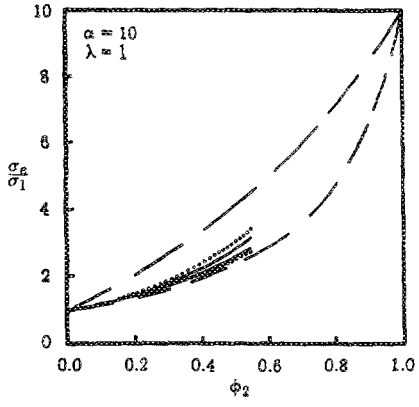


FIG. 10. As in Fig. 4, with $\lambda = 1.0$.

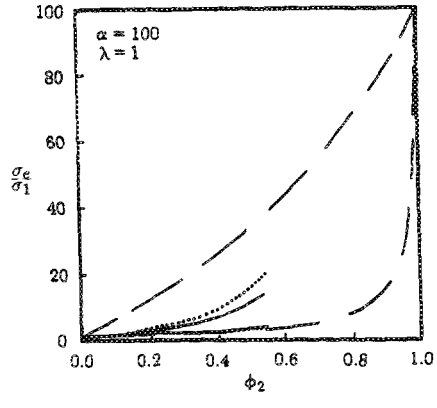


FIG. 11. As in Fig. 5, with $\lambda = 1.0$.

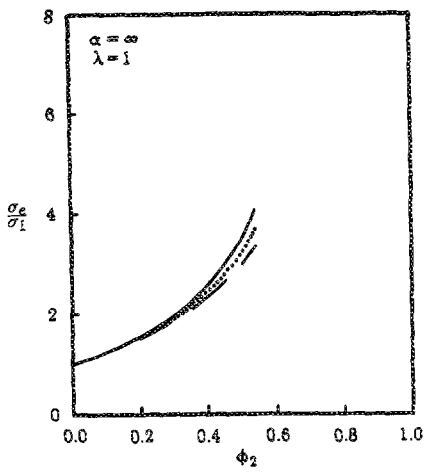


FIG. 12. As in Fig. 6, with $\lambda = 1.0$.

which are not expected to be drastically different from RSA thresholds. For $\lambda = 0.7$ and 0.9, $\phi_{2c} \approx 0.71$ and 0.77, respectively, for equilibrium simulations.[28] For $\alpha = \infty$, the upper bounds diverge to infinity; however, the fourth-order lower bound should still yield a good estimate of $\sigma_e/\sigma_1$ when $\Lambda_2 \ll L$. The results, in general, show that the effect of decreasing $\lambda$ at fixed $\phi_2$ is to increase the effective conductivity.

In Fig. 13, we compare the fourth-order bound on $\sigma_e/\sigma_1$ for $\alpha = 50$ to exact computer simulations of the effective conductivity for RSA of totally impenetrable cylinders

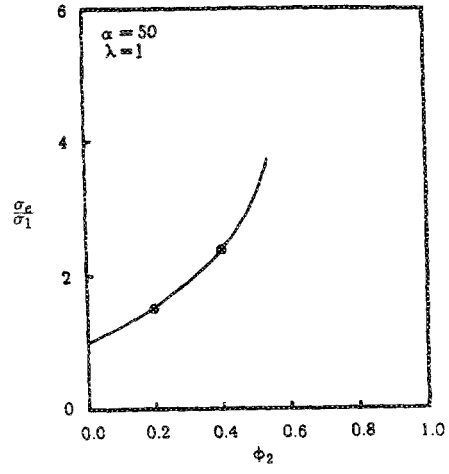


FIG. 13. Comparison of the fourth-order lower bound on the scaled conductivity to simulation results (solid circles) for the RSA distribution with $\lambda = 1$ and $\alpha = 50$ (see Ref. 21).

($\lambda = 1$) obtained recently by Durand and Ungar.[21] (These authors actually studied equilibrium distributions but for $\phi_2 \leqslant 0.4$ employed RSA distributions for reasons mentioned above.) The fourth-order lower bound, not surprisingly, is seen to predict the effective conductivity extremely accurately. This supports our assertion that bounds, which incorporate nontrivial microstructural information on the medium, can be employed to accurately estimate effective properties, even when the phase properties are widely different.

## ACKNOWLEDGMENTS

The authors gratefully acknowledge the support of the Office of Basic Energy Sciences, U.S. Department of Energy, under Grant No. DE-FG05-86ER13482. We would also like to thank the North Carolina State University Computing Center for providing substantial computing resources.

[1]Z. Hashin, J. Appl. Mech. **50**, 481 (1983).
[2]S. Torquato, Rev. Chem. Eng. **4**, 151 (1987).
[3]J. G. Berryman, J. Acoust. Soc. Am. **69**, 416 (1981).
[4]G. W. Milton, J. Appl. Phys. **52**, 5294 (1981).
[5]S. Torquato, J. Appl. Phys. **58**, 3790 (1985).
[6]Z. Hashin, in *Mechanics of Composite Materials*, edited by F. W. Wendt, H. Liebowitz, and N. Perrone (Pergamon, New York, 1970), p. 201.
[7]G. W. Milton, J. Mech. Phys. Solids **30**, 177 (1982).
[8]N. Silnutzer, Ph. D. thesis (University of Pennsylvania, Philadelphia, 1972).
[9]S. Torquato and G. Stell, J. Chem. Phys. **77**, 2071 (1982).
[10]S. Torquato and G. Stell, Lett. Appl. Eng. Sci. **23**, 375 (1985); S. Torquato and F. Lado, Phys. Rev. B **33**, 6428 (1986); S. Torquato and F. Lado, J. Appl. Mech. **55**, 347 (1988).
[11]S. Torquato and J. D. Beasley, Int. J. Eng. Sci. **24**, 415 (1986).
[12]S. Torquato and F. Lado, Proc. R. Soc. London Ser. A **417**, 59 (1988).
[13]J. P. Hansen and I. R. McDonald, *Theory of Simple Liquids* (Academic, New York, 1976).
[14]J. G. Berryman, J. Appl. Phys. **57**, 2374 (1985); J. Comput. Phys. **75**, 86 (1988).
[15]B. J. Alder, J. J. Weiss, and H. L. Strauss, Phys. Rev. A **7**, 281 (1973).
[16]P. Smith and S. Torquato, J. Comput. Phys. **76**, 176 (1988).
[17]S. Torquato, J. Chem. Phys. **81**, 5079 (1984); **84**, 6345 (1986).
[18]S. Kirkpatrick, Rev. Mod. Phys. **45**, 574 (1973).
[19]B. Widom, J. Chem. Phys. **44**, 3888 (1966); **58**, 4043 (1973).
[20]J. Feder, J. Theor. Biol. **87**, 237 (1980).
[21]P. P. Durand and L. H. Ungar, Int. J. Numer. Methods Eng. (in press).
[22]N. Metropolis, A. W. Rosenbluth, M. N. Rosenbluth, A. H. Teller, and E. Teller, J. Chem. Phys. **21**, 1087 (1953).
[23]J. M. Haile, C. Massobrio, and S. Torquato, J. Chem. Phys. **83**, 4075 (1985).
[24]S. B. Lee and S. Torquato, J. Chem. Phys. **89**, 3258 (1988).
[25]G. S. Fishman and L. R. Moore, J. Am. Stat. Assoc. **77**, 129 (1982).
[26]J. D. Beasley and S. Torquato, J. Appl. Phys. **60**, 3576 (1986).
[27]A. S. Sangani and C. Yao, Phys. Fluids **31**, 2426 (1988).
[28]S. B. Lee and S. Torquato, J. Chem. Phys. **89**, 6427 (1988).